

The synchrotron-self-Compton spectrum of relativistic blast waves at large Y

Martin Lemoine^{1*}

¹*Institut d'Astrophysique de Paris, CNRS, UPMC, 98 bis boulevard Arago, F-75014 Paris, France*

ABSTRACT

Recent analyses of multiwavelength light curves of gamma-ray bursts afterglows point to values of the magnetic turbulence well below the canonical $\sim 1\%$ of equipartition, in agreement with theoretical expectations of a micro-turbulence generated in the shock precursor, which then decays downstream of the shock front through collisionless damping. As a direct consequence, the Compton parameter Y can take large values in the blast. In the presence of decaying micro-turbulence and/or as a result of the Klein-Nishina suppression of inverse Compton cooling, the Y parameter carries a non-trivial dependence on the electron Lorentz factor, which modifies the spectral shape of the synchrotron and inverse Compton components. This paper provides detailed calculations of this synchrotron-self-Compton spectrum in this large Y regime, accounting for the possibility of decaying micro-turbulence. It calculates the expected temporal and spectral indices α and β customarily defined by $F_\nu \propto t_{\text{obs}}^{-\alpha} \nu^{-\beta}$ in various spectral domains. This paper also makes predictions for the very high energy photon flux; in particular, it shows that the large Y regime would imply a detection rate of gamma-ray bursts at > 10 GeV several times larger than currently anticipated.

Key words: acceleration of particles – shock waves – gamma-ray bursts: general

1 INTRODUCTION

The afterglow radiation of gamma-ray bursts, which spans the range from the radio domain to the X-ray and possible higher frequencies, with a characteristic decrease in time of the peak flux, is nicely interpreted in terms of the synchrotron radiation of ultra-relativistic electron that have been accelerated at the forward ultra-relativistic collisionless shock wave of the outflow, see e.g. Piran (2004) for a detailed review.

This model thus opens a beautiful connection between astronomical data and the microphysics of the rather extreme phenomena that relativistic collisionless shocks represent. Zooming in on microphysical scales reveals the shock front as a micro-turbulent magnetic barrier which isotropizes the incoming background plasma, see e.g. Moiseev & Sagdeev (1963) for pioneering studies and Kato & Takabe (2008), Spitkovsky (2008a) for detailed numerical simulations. This micro-turbulent barrier itself results from the build-up of electromagnetic micro-instabilities ahead of the shock front, in the shock precursor where supra-thermal particles mix with the incoming background plasma, e.g. Medvedev & Loeb (1999), Wiersma & Achterberg (2004), Lyubarksky & Eichler (2006), Achterberg & Wiersma (2007), Achterberg et al. (2007), Bret et al. (2010), Lemoine & Pelletier (2010, 2011), Rabinak et al. (2011), Shaisultanov et al. (2012), Lemoine et al. (2014a, b).

The resulting micro-turbulence, with typical length scale

$\lambda_{\delta B} \sim c/\omega_{\text{pi}}$ (ω_{pi} the ion plasma frequency) and typical strength¹ $\epsilon_B \sim 0.01$, thus emerges as a key ingredient for the microphysics of collisionless shocks. Actually, it also represents a key requisite for the relativistic Fermi process, since this latter can take place (in ideal conditions) only when an intense micro-turbulence, with power on scales smaller than the gyroradius of the accelerated particles, is able to unlock the particles off the background magnetic field lines, by scattering them faster than a gyration time in this background field (Lemoine et al. 2006, Niemiec et al. 2006, Pelletier et al. 2009). In terms of magnetization $\sigma = B^2 / (8\pi 4\Gamma_b^2 n m_p c^2)$, with B the background field expressed in the downstream frame, this condition amounts to $\sigma \ll \epsilon_B^2$ (Lemoine & Pelletier 2010, 2011, Lemoine et al. 2014a), a condition which is indeed satisfied for the forward shock of gamma-ray bursts, since $\sigma \sim 10^{-9}$ in the interstellar medium. This point of view has been confirmed by particle-in-cell simulations (e.g. Spitkovsky 2008b, Martins et al. 2009, Nishikawa et al. 2009, Sironi & Spitkovsky 2009, 2011, Sironi et al. 2013, Haugbølle 2011).

Finally, these micro-instabilities may also build the magnetized turbulence in which the electrons eventually produce the afterglow radiation in a synchrotron-like process (Medvedev & Loeb 1999) – jitter effects are expected to be weak in the conditions

¹ $\epsilon_B \equiv \delta B^2 / (8\pi 4\Gamma_b^2 n m_p c^2)$ represents the magnetic energy fraction of equipartition, if $\Gamma_b \gg 1$ represents the relative Lorentz factor between upstream and downstream, n the upstream proper density.

* e-mail:lemoine@iap.fr

typical of those shock waves – provided it survives collisionless damping downstream of the shock front (Gruzinov & Waxman 1999). Recent analyses of the damping of this Weibel-type micro-turbulence yield a damping rate $\propto k^3$, where k denotes a turbulent wavenumber, indicating that small scales are dissipated first, but that large scales may survive longer (Chang et al. 2008, Lemoine 2015). In turn, this implies that the turbulence strength, or ϵ_B , should decay as a power-law in (proper) time (or distance) downstream of the shock front, with an index which itself depends on the (unknown) micro-turbulent power spectrum at the shock front. Interestingly, this time dependence of ϵ_B turns out to be encoded in the multiwavelength synchrotron spectrum, since electrons of different Lorentz factors cool at different times, hence in regions of different magnetic field strengths (Rossi & Rees 2003, Derishev 2007, Lemoine 2013).

Although one cannot exclude that other external instabilities would pollute the blast with magnetized turbulence, it is tempting to consider that the generation of micro-turbulence could be responsible at the same time for the formation of the shock, for the acceleration of particles and for the radiation of these particles. It is furthermore tempting to follow this thread to use the multiwavelength spectrum of gamma-ray bursts as a tomograph of the magnetized turbulence. As a matter of fact, the recent detections of extended emission of gamma-ray bursts in the > 100 MeV band by the Fermi-LAT instrument do point to a net decay of the micro-turbulence behind the shock front (Lemoine et al. 2013), with $\epsilon_B \propto (t\omega_{\text{pi}}/100)^{\alpha_t}$ and $-0.5 \lesssim \alpha_t \lesssim -0.4$. This argument can be recapped as follows: if the accelerated particles scatter in a micro-turbulence, the maximal synchrotron photon energy is limited to a few GeV at an observer time of 100 s (Kirk & Reville 2010, Plotnikov et al. 2013, Wang et al. 2013, Sironi et al. 2013); this maximal energy scales as the square root of ϵ_{B+} , i.e. the magnitude of the turbulence in the vicinity of the shock front, and the above value assumes $\epsilon_{B+} = 0.01$; therefore, the interpretation of this extended > 100 MeV emission as a synchrotron process points to the existence of a strong micro-turbulence close to the shock front; on the other hand, multiwavelength fits of the afterglows for these Fermi-LAT gamma-ray bursts indicate that low-energy photons are produced in regions of rather low ϵ_{B-} , of the order of $10^{-6} - 10^{-5}$; this discrepancy between ϵ_{B-} and ϵ_{B+} is naturally interpreted as the decay of the micro-turbulence through collisionless damping. As discussed in Lemoine et al. (2013), the decay rate $\alpha_t \sim -0.5$ to -0.4 further matches the results of a detailed numerical experiment reported in Keshet et al. (2009).

The decay of micro-turbulence has also been proposed as a possible solution to the abnormal spectral indices observed in the prompt emission phase (Derishev 2007), but admittedly, the physics of mildly relativistic shock waves may well differ from that of ultra-relativistic shock waves; in particular, the extended precursor size in mildly relativistic shocks opens the way to other instabilities operating on larger length scales. Although the present considerations can also be generalized to the case of internal shocks, all of the discussion that follows will focus on the external ultra-relativistic shock front.

An interesting consequence of a decaying micro-turbulence, or more generally, of a low average value of ϵ_B as measured in the Fermi-LAT and other bursts (e.g. Kumar & Barniol-Duran 2009, 2010, He et al. 2011, Santana et al. 2014, Barniol-Duran 2014), is a large Compton parameter Y , at least if one omits the influence of Klein-Nishina effects, which actually depend on electron energy hence on observed frequency, see below. Recall indeed that in the standard model, assuming that electrons cool through in-

verse Compton interactions on their synchrotron spectrum in the Thomson limit (i.e. neglecting Klein-Nishina – KN – effects), $Y \sim (\eta\epsilon_e/\epsilon_B)^{1/2}$ at $Y \gg 1$, with $\eta \simeq \min[1, (\gamma_c/\gamma_m)^{2-p}]$ the cooling efficiency of electrons, γ_c denoting the Lorentz factor of electrons which cool on a dynamical timescale, γ_m the minimum Lorentz factor of the injected electron power-law and $-p$ the index of this power-law, e.g. Panaitescu & Kumar (2000), Sari & Esin (2001), Piran (2004). This Y parameter also reflects the power of the inverse Compton component relatively to the synchrotron component, therefore the ratio of emission at very high energies to that in the X-ray range. The possibility of a large Y parameter should thus increase the chances of observing gamma-ray bursts at very high energies with upcoming Čerenkov telescopes. The observation of this inverse Compton component would then open a new spectral domain with which one could study the microphysics of the turbulence in the blast.

However, the computation of the synchrotron-self Compton (SSC) spectrum of the blast in the large Y regime is not trivial because the shape of the synchrotron spectrum influences the cooling history of the electrons, which itself determines the synchrotron spectral shape. In particular, the KN suppression of the inverse Compton cross-section may itself modify this cooling history, hence modify the very shape of the synchrotron spectrum, see Nakar et al. (2009), Wang et al. (2010); see also Barniol Duran & Kumar (2011) for the particular case of GRB090902B and Bošnjak et al. (2009), Daigne et al. (2011) for related discussions in the context of gamma-ray burst prompt emission. In the case of decaying micro-turbulence, this issue is more acute, because the synchrotron power νF_ν may be rising with frequency, due to the fact that lower frequency photons are emitted by electrons of longer cooling time, in regions of lower magnetic field strength (Lemoine 2013). Therefore, the Lorentz factor-dependent KN limit determines the radiation intensity on which an electron can cool. Finally, so far the influence of decaying micro-turbulence on the synchrotron spectrum has been studied for a fixed Y parameter, independent of electron Lorentz factor, hence the general shape of the SSC spectrum is not known in this physically relevant case.

These considerations motivate the present study, which calculates the SSC spectrum for a relativistic blast wave in the large Y regime. Although the prime objective is to understand how the decaying micro-turbulence affects the SSC spectrum, the present discussion also addresses the case of a uniform, low value of ϵ_B . The results are applied to the case of the GRB afterglows, by calculating the spectrum at various observer time and by plotting, in particular, the spectral slopes in various frequency windows. The spectrum is also evaluated in the multi-GeV range, with a proper account of synchrotron and SSC contributions, to make clear predictions for future Čerenkov observatories such as HAWK and CTA.

This paper is organized as follows: Sec. 2 presents an analytical description of the spectrum in the slow-cooling limit, accounting for KN effects, and introduces a fast algorithm to compute this spectrum in the fast cooling regime; Sec. 3 then computes the light curves and plots the temporal and spectral indices α and β , commonly defined by $F_\nu \propto t_{\text{obs}}^{-\alpha} \nu^{-\beta}$, and gives predictions for the very high energy photon flux; finally, Sec. 4 summarizes these results and provides some conclusions.

2 SSC SPECTRUM

2.1 Set-up

The set-up is as follows: electrons are swept-up by a relativistic shock front propagating in a density profile $n \propto r^{-k}$, then accelerated on a short time-scale to a power-law $dN_{e,0}/d\gamma \propto \gamma^{-p}\Theta(\gamma - \gamma_m)$ above a minimal Lorentz factor γ_m . The minimal Lorentz factor is defined as usual by $\gamma_m \equiv \epsilon_e \Gamma_b m_p / m_e (p - 2) / (p - 1)$, with $\epsilon_e \sim 0.1$. Cooling takes place on much longer timescales. When describing the cooling history, the total inverse Compton cross-section is modelled as a top-hat, with $\sigma = \sigma_T$ for $\nu < \tilde{\nu}(\gamma)$ and zero otherwise, $\tilde{\nu}(\gamma)$ denoting the frequency of photons with which electrons of Lorentz factor γ interact at the KN limit (Nakar et al. 2009, Wang et al. 2010), i.e.

$$\tilde{\nu} \equiv \frac{\Gamma_b m_e c^2}{h\gamma(1+z)}. \quad (1)$$

All frequencies are written in the observer rest frame; as mentioned above, Γ_b denotes the Lorentz factor of the blast in the source rest frame. The Compton parameter can then be approximated as

$$Y(\gamma) \simeq \frac{U_{\text{rad}}[\nu < \tilde{\nu}(\gamma)]}{U_B(\gamma)}, \quad (2)$$

where

$$U_{\text{rad}}[\nu < \tilde{\nu}(\gamma)] = \int_0^{\tilde{\nu}(\gamma)} d\nu U_\nu(\nu) \quad (3)$$

represents the comoving radiation energy density at frequencies $\nu < \tilde{\nu}(\gamma)$, on which the electron of Lorentz factor γ can cool. Of course, if $\tilde{\nu} > \nu_{\text{peak}}$ at which the differential energy density $U_\nu(\nu)$ reaches its maximum, then $U_{\text{rad}}[\nu < \tilde{\nu}(\gamma)] \sim \nu_{\text{peak}} U_{\nu_{\text{peak}}} \sim U_{\text{rad}}$ and it does not depend on γ (U_{rad} denotes here the total comoving energy density). In principle, U_{rad} includes all form of radiation, synchrotron and inverse Compton alike; however, multiple Compton scattering can be neglected for standard gamma-ray bursts parameters, hence U_{rad} is hereafter determined with the synchrotron spectrum only.

The quantity $U_B(\gamma)$ represents the energy density contained in the magnetic field and it depends on γ if the turbulence decays in (proper) time behind the shock, because electrons of different Lorentz factors then cool in regions of different magnetic field strengths. In this work, the decay law of the turbulence takes the power-law form $\epsilon_B(t) \propto t^{\alpha_t}$ far from the shock front and $\epsilon_B \sim \epsilon_{B+} = 0.01$ close to the shock front. How far is expressed in terms of the proper time t since the plasma element was injected through the shock, i.e. $t \equiv x/\beta_d$ in terms of the downstream (comoving) distance to the shock front x and β_d , the shock front velocity relative to the downstream rest frame. According to PIC simulations, the characteristic (temporal) scale Δ separating far from close to the shock front is $\Delta \sim 10^{2-3} \omega_{\text{pi}}$, see Chang et al. (2008), Keshet et al. (2009) for simulations, as well as Lemoine (2013), Lemoine (2015) for discussions of this issue; for reference, $\omega_{\text{pi}}^{-1} \sim 7.5 \times 10^{-4} n_0^{-1/2}$ s for a relativistic blast wave propagating in a medium of proton density $n_0 \text{ cm}^{-3}$. The uncertainty on the value of Δ does not really influence the results presented below, because it can be embedded in that associated to the decay power-law exponent α_t . Recent work mentioned above suggest $\alpha_t \sim -0.5 \rightarrow -0.4$ for a decay law $\epsilon_B \sim \epsilon_{B+} (t\omega_{\text{pi}}/100)^{\alpha_t}$, hence the following adopts $\Delta = 100\omega_{\text{pi}}^{-1}$ and $\alpha_t = -0.4$. This decay implies that the minimum magnetic field in the blast, close to the contact discontinuity, is characterized by the equipartition fraction $\epsilon_{B-} = \epsilon_{B+} (t_{\text{dyn}}/\Delta)^{\alpha_t}$ in terms of the dynamical timescale

$t_{\text{dyn}} = r/(\Gamma_b c)$. Typical values are $t_{\text{dyn}} \sim 10^5 - 10^6$ s at an observer time of 10^4 s (e.g. $\Gamma_b \sim 20 - 30$ and $r \sim 10^{17} - 10^{18}$ cm), with a mild dependence on the model parameters, leading to values of the order of $\epsilon_{B-} \sim 10^{-5}$ for $\alpha_t \sim -0.5$. Note that $t_{\text{dyn}}/\Delta \propto t_{\text{obs}}^{(5-2k)/(8-2k)}$ evolves slowly as a function of observer time, hence so does ϵ_{B-} .

In this work, it is assumed that a particle emits its synchrotron radiation at the location at which it cools, if it cools on a dynamical timescale; in the opposite limit, it is assumed that it emits its synchrotron photons in the magnetic field close to the contact discontinuity, of strength δB_- (associated to the parameter ϵ_{B-}). The justification of this approximation is as follows: the energy emitted in synchrotron photons by a particle up to time t , along its trajectory downstream of the shock, can be written as

$$E_{\text{syn}} = \frac{1}{6\pi} \sigma_T c \int_0^t d\tau \delta B^2(\tau) \gamma_e^2(\tau) \beta_e^2(\tau) \quad (4)$$

as a function of the time dependent Lorentz factor $\gamma_e(\tau)$ of the particle along its cooling trajectory, with $\beta_e(\tau) \sim 1$ the particle velocity in units of c . One can then show that E_{syn} is dominated by the contribution at $t \sim t_{\text{cool}}(\gamma)$, where γ denotes the initial value $\gamma_e(0)$, as follows. At early times $\tau \ll t_{\text{cool}}(\gamma)$, $\gamma_e(\tau) \sim \gamma$ and the integrand scales as $U_B(\tau) \propto \tau^{\alpha_t}$, hence the integral is dominated by the large time behavior if $\alpha_t > -1$, which is indeed an explicit assumption of the present work. At late times $\tau \gg t_{\text{cool}}(\gamma)$, one can obtain an upper bound on how fast $\gamma_e(\tau)$ decreases by considering synchrotron losses only, i.e. by neglecting inverse Compton losses. The integration of

$$\frac{d\gamma_e}{d\tau} = -\frac{4}{3} \frac{\sigma_T c U_B(\tau)}{m_e c^2} \gamma_e^2(\tau) \beta_e(\tau)^2 \quad (5)$$

leads to $\gamma_e(\tau) \sim \gamma [\tau/t_{\text{cool}}(\gamma)]^{-1-\alpha_t}$ for $\tau \gg t_{\text{cool}}(\gamma)$. Therefore, the integrand in Eq. (4) behaves as $\tau^{-2-\alpha_t}$ for $\tau > t_{\text{cool}}(\gamma)$, hence E_{syn} is indeed dominated by the contribution at $t \sim t_{\text{cool}}(\gamma)$ provided $\alpha_t > -1$.

This thus supports the above approximation that a particle with initial Lorentz factor $\gamma > \gamma_c$ emits its synchrotron radiation on a magnetic field of strength $\delta B [t_{\text{cool}}(\gamma)]$, with $t_{\text{cool}}(\gamma)$ the cooling time of the particle. Of course, if $t_{\text{cool}}(\gamma) > t_{\text{dyn}}$, the particle does not actually cool, and E_{syn} is then dominated by the upper bound $t \sim t_{\text{dyn}}$, i.e. particles radiate synchrotron radiation in the relaxed magnetic field at the back of the blast, of strength δB_- .

Since $t_{\text{cool}}(\gamma_c) = t_{\text{dyn}}$ by definition, and since $\delta B(t_{\text{dyn}}) = \delta B_-$, also by definition,

$$U_B(\gamma) \simeq U_{B-} \max \left[1, \left(\frac{t_{\text{cool}}(\gamma)}{t_{\text{dyn}}} \right)^{\alpha_t} \right] \quad (6)$$

with $U_{B-} \equiv \delta B_-^2 / (8\pi) = U_B(\gamma_c)$.

In line with the above discussion, electrons of Lorentz factor γ radiate their energy through synchrotron at a typical frequency

$$\nu_{\text{syn}}(\gamma) \propto \delta B [t_{\text{cool}}(\gamma)] \gamma^2 \simeq \nu_c \left[\frac{t_{\text{cool}}(\gamma)}{t_{\text{dyn}}} \right]^{\alpha_t/2} \left(\frac{\gamma}{\gamma_c} \right)^2. \quad (7)$$

Here, $\nu_c \equiv \nu_{\text{syn}}(\gamma_c)$ denotes the synchrotron peak frequency for particles of Lorentz factor γ_c .

Finally, the cooling timescale can be written

$$\begin{aligned} t_{\text{cool}}(\gamma) &\simeq t_{\text{dyn}} \frac{1 + Y_c}{1 + Y(\gamma)} \frac{U_{B-}}{U_B(\gamma)} \frac{\gamma_c}{\gamma}, \\ &\simeq t_{\text{dyn}} \left[\frac{1 + Y(\gamma)}{1 + Y_c} \right]^{-1/(1+\alpha_t)} \left(\frac{\gamma}{\gamma_c} \right)^{-1/(1+\alpha_t)} \end{aligned} \quad (8)$$

The second equality is obtained by replacing $U_B(\gamma)/U_{B-}$ with its value given in Eq. (6), assuming $\gamma > \gamma_c$.

Equations (2), (6), (7) and (8) then allow to derive the following scalings for $\gamma > \gamma_c$:

$$\frac{U_B(\gamma)}{U_{B-}} \simeq \left[\frac{1+Y(\gamma)}{1+Y_c} \right]^{-\alpha_t/(1+\alpha_t)} \left(\frac{\gamma}{\gamma_c} \right)^{-\alpha_t/(1+\alpha_t)}, \quad (9)$$

$$\frac{\nu_{\text{syn}}(\gamma)}{\nu_c} \simeq \left[\frac{1+Y(\gamma)}{1+Y_c} \right]^{-\alpha_t/[2(1+\alpha_t)]} \left(\frac{\gamma}{\gamma_c} \right)^{2-\alpha_t/[2(1+\alpha_t)]}, \quad (10)$$

$$\frac{Y(\gamma) [1+Y(\gamma)]^{-\alpha_t/(1+\alpha_t)}}{Y_c(1+Y_c)^{-\alpha_t/(1+\alpha_t)}} \simeq \frac{U_{\text{rad}}(\nu < \tilde{\nu})}{U_{\text{rad}}(\nu < \tilde{\nu}_c)} \left(\frac{\gamma}{\gamma_c} \right)^{\alpha_t/[1+(1+\alpha_t)]}. \quad (11)$$

Y_c stands for $Y(\gamma_c)$.

Once the ratio $U_{\text{rad}}(\nu < \tilde{\nu})/U_{\text{rad}}(\nu < \tilde{\nu}_c)$ – which captures KN effects – has been specified, it is possible to derive the scalings of $Y(\gamma)$ as a function of γ , hence of $\nu_{\text{syn}}(\gamma)$. One should emphasize that in the above expressions, γ represents the initial Lorentz factor of the particle, after acceleration has shaped the power-law, but before cooling has effectively taken place.

2.2 Synchrotron spectrum

Standard calculations of the synchrotron spectrum of a blast wave generally derive the stationary electron distribution in the blast, by solving a transport equation in momentum space, averaged over the depth of the blast, accounting for injection of the power-law at the shock and for cooling downstream (e.g. Sari et al. 1998, Sari & Esin 2001); this yields a standard broken power-law shape $dN_e/d\gamma_e$ with indices -2 for $\gamma_c < \gamma < \gamma_m$ or $-p$ for $\gamma_m < \gamma < \gamma_c$ and $-p-1$ for $\max(\gamma_c, \gamma_m) < \gamma$. However, one can also derive the synchrotron spectrum by a direct mapping of the energy initially stored into the electron population to that radiated in synchrotron; this approach is simpler in the present case and it works as follows.

Electrons injected with Lorentz factor $\gamma > \max(\gamma_m, \gamma_c)$ emit a fraction $[1+Y(\gamma)]^{-1}$ of their energy in synchrotron radiation; the energy density contained in such electrons (within an interval $d \ln \gamma$) is itself a fraction $(p-2)(\gamma/\gamma_m)^{2-p} d \ln \gamma$ of the energy density U_e contained in electrons immediately behind the shock front, before cooling has started to take place; $U_e = \epsilon_e 4\Gamma_b^2 n m_p c^2$. Consequently, the synchrotron flux received at frequency $\nu = \nu_{\text{syn}}(\gamma)$ can be written:

$$\nu F_{\nu, \text{syn}} \simeq \frac{1}{4\pi D_L^2} \frac{4}{3} \Gamma_b^2 \frac{4\pi r^2 c(p-2)U_e}{1+Y(\gamma)} \left(\frac{\gamma}{\gamma_m} \right)^{2-p} \frac{d \ln \gamma}{d \ln \nu} \quad (12)$$

The above assumes $p > 2$, but it can be generalized to any index $p > 1$; indeed, the above picture assumes that particles with $\gamma > \max(\gamma_m, \gamma_c)$ radiate their energy at $\nu_{\text{syn}}(\gamma)$ then do not contribute anymore to the synchrotron spectrum, which is a reasonable approximation if $p > 1$; in contrast, if $p < 1$, the radiation of the high energy particles during their complete cooling history dominates that of the lower energy ones.

Similarly, one can write down the flux for $\gamma_m > \gamma > \gamma_c$ or $\gamma_c > \gamma > \gamma_m$, whichever occurs, as follows:

$$\nu F_{\nu, \text{syn}} \simeq \nu_m F_{\nu_m, \text{syn}} \begin{cases} \frac{\gamma}{\gamma_m} \frac{1+Y_m}{1+Y} & (\gamma_m > \gamma > \gamma_c) \\ \left(\frac{\nu}{\nu_m} \right)^{(3-p)/2} & (\gamma_c > \gamma > \gamma_m) \end{cases} \quad (13)$$

with $Y_m \equiv Y(\gamma_m)$ and $\nu_m = \nu_{\text{syn}}(\gamma_m)$. The spectrum at $\nu < \nu_c$ is indeed unchanged with respect to the standard case, although the value of U_{B-} must be used to compute the characteristic frequencies. Regarding the fast cooling limit $\gamma_c < \gamma < \gamma_m$, the factor can be understood by noting that all injected particles with $\gamma > \gamma_m$ shift from γ to γ_c during their cooling history, and that at each point along this cooling trajectory they radiate (in synchrotron) a fraction $(\gamma/\gamma_m)(1+Y_m)/(1+Y)$ of the energy radiated (in synchrotron) by a particle of Lorentz factor γ_m . Note also that in the limits $\alpha_t \rightarrow 0$, $Y(\gamma) \ll 1$, one recovers the usual scaling $\nu F_{\nu, \text{syn}} \propto \nu^{1/2}$ since $\nu \propto \gamma^2$.

Provided γ_c and Y_c are given, one can derive $\nu_{\text{syn}}(\gamma)$ and $Y(\gamma)$, hence $\gamma(\nu)$ and $Y(\nu)$ by using Eqs. (9), (10) and (11), then $\nu F_{\nu, \text{syn}}$ using Eqs. (12) and (13). Consider as an example the case $Y \gg 1$, omitting KN effects, i.e. $\tilde{\nu} \rightarrow +\infty$ for all ν : for $\gamma > \gamma_c$, one derives $Y(\gamma) \propto \gamma^{\alpha_t}$ from Eq. (11), hence $\nu_p \propto \gamma^{2-\alpha_t/2}$ from Eq. (10), hence $\nu F_{\nu, \text{syn}} \propto \gamma^{2-p}/(1+Y) \propto \nu^{(2-p-\alpha_t)/(2-\alpha_t/2)}$ from Eq. (12). This latter scaling matches the explicit calculation of Lemoine (2013), which computes the integrated cooling history of the electron power-law in the decaying magnetic field. This example also confirms that $\nu F_{\nu, \text{syn}}$ rises with ν if $\alpha_t \lesssim 2-p$, hence KN effects should not be omitted in an accurate calculation of $\nu F_{\nu, \text{syn}}$.

The above provides the tools needed to calculate the synchrotron spectrum; explicit calculations in both the slow and the fast cooling regimes are provided in the following sections.

2.3 Inverse Compton spectrum

In order to calculate the inverse Compton emissivity, the synchrotron spectral density $F_{\nu, \text{syn}}$ must be folded over the Compton cross-section and the cooled particle distribution, integrated over the blast. The following derivation of the cooled distribution function relies on the observations that $dt_{\text{cool}}(\gamma)/d\gamma < 0$ and that the cooling history $\gamma_{\text{cool}}(t)$ at times $t > t_0$ does not depend on the history at times $t < t_0$, i.e. electrons of various Lorentz factor follow a universal cooling trajectory $\gamma_{\text{cool}}(t)$.

One writes $d\dot{N}_{e,0}$ the (comoving) rate at which electrons are swept-up and accelerated into a power-law in a Lorentz factor interval $d\gamma$. One also defines dN_e , which represents the total number of electrons in the blast in a Lorentz factor interval $d\gamma_e$; note the difference of notation: γ_e refers to a value of the Lorentz factor of the blast averaged distribution, while γ corresponds to the Lorentz factor of the injection distribution, i.e. before cooling has occurred.

The injection of particles with Lorentz factor γ populates the downstream with particles of Lorentz factor $\gamma_e = \gamma$ over a fraction $t_{\text{cool}}/t_{\text{dyn}}$ of the depth of the blast. In contrast, particles injected with $\gamma_c > \gamma > \gamma_m$ retain their Lorentz factor (no cooling) and populate the whole blast. Therefore, one can write the average distribution for $\gamma_e > \gamma_m$ as:

$$\frac{dN_e}{d\gamma_e} \simeq \frac{d\dot{N}_{e,0}}{d\gamma} (\gamma = \gamma_e) \min[t_{\text{dyn}}, t_{\text{cool}}(\gamma)] \quad (\gamma > \gamma_m). \quad (14)$$

Note also that t_{dyn} sets the scale for adiabatic losses, while t_{cool} sets the scale for radiative losses.

In the fast cooling regime, all electrons injected with Lorentz factor $\gamma > \gamma_m$ cool down to γ_c , following a same cooling history

$\gamma_{\text{cool}}(\tau)$, therefore

$$\begin{aligned} \frac{dN_e}{d\gamma_e} &\simeq \int_0^{t_{\text{dyn}}} d\tau \int_{\gamma_m}^{+\infty} d\gamma \frac{d\dot{N}_{e,0}}{d\gamma} \delta[\gamma_e - \gamma_{\text{cool}}(\tau)] \\ &\simeq \dot{N}_{e,0} \frac{t_{\text{cool}}(\gamma_e)}{\gamma_e} \end{aligned} \quad (15)$$

where $\dot{N}_{e,0} = \int_{\gamma_m}^{+\infty} d\gamma d\dot{N}_{e,0}/d\gamma$ represents the total injection rate of electrons. The last expression in Eq. (15) follows from the definition $t_{\text{cool}}(\gamma_e) = \gamma_e |d\gamma_e/dt|^{-1}$ after interchanging the integrals.

Using the scaling of $t_{\text{cool}}(\gamma)$, one then derives

$$\begin{aligned} \frac{dN_e}{d\gamma_e} &\simeq \frac{\dot{N}_{e,0} t_{\text{dyn}}}{\gamma_m} \left(\frac{\gamma_e}{\gamma_m} \right)^{-p} \quad (\gamma_m < \gamma_e < \gamma_c) \\ \frac{dN_e}{d\gamma_e} &\simeq \frac{\dot{N}_{e,0} t_{\text{dyn}}}{\gamma_m} \left(\frac{\gamma_e}{\gamma_m} \right)^{-1} \left(\frac{\gamma_e}{\gamma_c} \right)^{-1/(1+\alpha_t)} \\ &\quad \times \left[\frac{1+Y(\gamma_e)}{1+Y_c} \right]^{-1/(1+\alpha_t)} \quad (\gamma_c < \gamma_e < \gamma_m) \\ \frac{dN_e}{d\gamma_e} &\simeq \frac{\dot{N}_{e,0} t_{\text{dyn}}}{\gamma_m} \left(\frac{\gamma_e}{\gamma_m} \right)^{-p} \left(\frac{\gamma_e}{\gamma_c} \right)^{-1/(1+\alpha_t)} \\ &\quad \times \left[\frac{1+Y(\gamma_e)}{1+Y_c} \right]^{-1/(1+\alpha_t)} \quad [\max(\gamma_c, \gamma_m) < \gamma_e] \end{aligned} \quad (16)$$

In the limit $\alpha_t \rightarrow 0$, one recovers $dN_e/d\gamma_e \propto [1+Y(\gamma_e)]^{-1} \gamma_e^{-2}$ for $\gamma_c < \gamma_e < \gamma_m$ or $dN_e/d\gamma_e \propto [1+Y(\gamma_e)]^{-1} \gamma_e^{-p-1}$ for $\gamma_m < \gamma_c < \gamma_e$; both match the expressions derived in Nakar et al. (2009) and in Wang et al. (2010) for a homogeneous (non-decaying) turbulence.

It is also instructive to show that the above average electron distribution, when associated with the appropriate (i.e. Lorentz factor dependent) magnetic field, leads to the same scalings for the synchrotron spectrum as Eqs. (12) and (13). Consider for instance the regime $\gamma > \max(\gamma_c, \gamma_m)$: the average synchrotron power of the blast scales as $\nu F_{\nu, \text{syn}} \propto U_B(\gamma_e) \gamma_e^2 dN_e/d \ln \gamma_e$; using the scaling for $U_B(\gamma_e)$ given in Eq. (9), one recovers $\nu F_{\nu, \text{syn}} \propto [1+Y(\gamma_e)]^{-1} \gamma_e^{2-p}$ indicated in Eq. (12). One can proceed similarly for the other two regimes, noting in particular that for $\gamma_m < \gamma_e < \gamma_c$ (slow cooling), $U_B = U_{B-}$ and it no longer depends on γ_e .

Finally, using the above electron distribution, one can compute the inverse Compton component using standard formulae:

$$\begin{aligned} F_{\nu, \text{IC}}(\nu_{\text{IC}}) &\simeq \tau_{\text{IC}} \int d\gamma_e \frac{1}{N_e} \frac{dN_e}{d\gamma_e} \int_0^1 dq (1-u) g_{\text{KN}}(q) \\ &\quad \times F_{\nu, \text{syn}} \left[\frac{\nu_{\text{IC}}}{4\gamma^2 q(1-u)} \right] \Theta(1-u), \end{aligned} \quad (17)$$

with $u \equiv (1+z)h\nu_{\text{IC}}/(\Gamma_b \gamma_e m_e c^2)$; the function $g_{\text{KN}}(q) = [2q \ln q + (1+2q)(1-q) + G^2(1-q)/[2(1+G)]]$, with $G \equiv u/(1-u)$ characterizes the energy dependence of the Klein-Nishina cross-section, see Blumenthal & Gould (1970) for details.

The prefactor τ_{IC} defines the optical depth to Compton scattering; an explicit calculation leads to

$$\tau_{\text{IC}} = 3\sigma_{\text{T}} \frac{N_e}{4\pi r^2} = 12\sigma_{\text{T}} \Gamma_b n c t_{\text{dyn}} \quad (18)$$

Note that this expression uses $N_e = 4\pi r^2 c t_{\text{dyn}} 4\Gamma_b n$, i.e. it only includes the electrons that have been swept up in the last dynamical

timescale, because electrons injected at earlier times have been adiabatically cooled to Lorentz factors $< \gamma_c$ and therefore do not participate in shaping the inverse Compton spectrum. With the above value of τ_{IC} , one can verify that the energy density of the radiation associated to the inverse Compton component is correctly normalized to Y_c times that contained in the synchrotron component, as can be verified by calculating $\int d\nu_{\text{IC}} F_{\nu_{\text{IC}}, \text{IC}}$ in terms of $\int d\nu_{\text{syn}} F_{\nu_{\text{syn}}, \text{syn}}$ (neglecting the influence of Klein-Nishina effects).

2.4 Slow cooling

2.4.1 General procedure

As discussed in detail in Nakar et al. (2009) and Wang et al. (2010), the cooling Lorentz factors and Compton parameters γ_c and Y_c can be obtained in the slow cooling regime $\gamma_m < \gamma_c$ from the system

$$\begin{aligned} Y_c(1+Y_c) &\simeq \frac{\epsilon_e}{\epsilon_{B-}} \left(\frac{\gamma_c}{\gamma_m} \right)^{2-p} \frac{U_{\text{syn}}(< \tilde{\nu}_c)}{U_{\text{syn}}(< \nu_c)} \\ \gamma_c &\simeq \frac{\gamma_{c, \text{syn}}}{1+Y_c} \end{aligned} \quad (19)$$

with $\gamma_{c, \text{syn}} \equiv (3/4)m_e c/(\sigma_{\text{T}} U_{B-} t_{\text{dyn}})$ the cooling Lorentz factor in the relaxed turbulence, in the absence of inverse Compton losses.

Write $C_c \equiv U_{\text{syn}}(< \tilde{\nu}_c)/U_{\text{syn}}(\nu_c)$ the term entering the first equation. If $\tilde{\nu}_c < \nu_c$, $C_c < 1$ because the peak of the synchrotron flux lies at ν_c or above (see below); in this limit, Klein-Nishina suppression inhibits the cooling of γ_c electrons. Assuming that such electrons cool by interacting with the $\nu_{\text{min}} < \nu < \nu_c$ part of the synchrotron spectrum, which is generically the case, one can write $C_c = (\tilde{\nu}_c/\nu_c)^{(3-p)/2} \propto \gamma_c^{-3(3-p)/2}$ and the system can be solved easily.

In the opposite limit, $\tilde{\nu}_c > \nu_c$; one may have $C_c \sim 1$ if the peak of the synchrotron flux is located at ν_c , or $C_c \gtrsim 1$ if the peak lies at higher frequencies. In this latter case, $C_c \simeq (\tilde{\nu}_c/\nu_c)^{1-\beta}$, where β is the synchrotron spectral index defined by $F_{\nu, \text{syn}} \propto \nu^{-\beta}$ in the spectral range above ν_c , calculated thereafter. The analytical calculation proposed here uses Eq. (27) below to derive this β , but the result depends little on this choice, because in all cases considered, $1-\beta$ is small, meaning that the peak flux is not very different from the flux νF_{ν} at ν_c .

The next step is to determine the critical Lorentz factors $\hat{\gamma}_c \equiv \hat{\gamma}(\nu_c)$ and $\hat{\gamma}_m \equiv \hat{\gamma}(\nu_m)$ with the general definition (Nakar et al. 2009):

$$\hat{\gamma}(\nu) = \frac{\Gamma_b m_e c^2}{(1+z)h\nu}, \quad (20)$$

which corresponds to the Lorentz factor for which electrons interact with photons of frequency ν at the onset of the Klein-Nishina regime. Note that ν_m and ν_c are to be calculated in the relaxed turbulence of strength δB_- in this slow cooling regime. Using Eqs. (9), (10) and (11), one may then calculate the Compton parameters $Y(\hat{\gamma}_c)$ and $Y(\hat{\gamma}_m)$. Note also that the slow cooling limit $\gamma_m < \gamma_c$ implies $\hat{\gamma}_c < \hat{\gamma}_m$.

Another critical Lorentz factor is γ_0 , for which $Y(\gamma_0) = 1$. If $Y(\hat{\gamma}_m) > 1$, then $\hat{\gamma}_m < \gamma_0$, and γ_0 can be obtained by solving

$$\frac{Y(\gamma_0) [1+Y(\gamma_0)]^{-\alpha_t/(1+\alpha_t)}}{Y(\hat{\gamma}_m) [1+Y(\hat{\gamma}_m)]^{-\alpha_t/(1+\alpha_t)}} = \left[\frac{\tilde{\nu}(\gamma_0)}{\nu_m} \right]^{4/3} \left(\frac{\gamma_0}{\gamma_m} \right)^{\alpha_t/(1+\alpha_t)} \quad (21)$$

which derives from Eq. (11). This latter equation assumes that

$\tilde{\nu}(\gamma_0)$ lies in the spectral range between ν_a (synchrotron self-absorption frequency) and ν_m , in general a very good approximation; it can be generalized to other cases without difficulty. If $Y(\hat{\gamma}_m) < 1$, then $\gamma_0 < \hat{\gamma}_m$; one can repeat the above exercise to derive γ_0 , replacing the $4/3$ exponents with $(3-p)/2$, which characterizes the spectral dependence of $\nu F_{\nu, \text{syn}}$ between ν_m and ν_c .

For improved accuracy, one may also determine the next order critical Lorentz factor $\hat{\gamma}_c \equiv \Gamma_b m_e c^2 / [(1+z)h\nu_{\text{syn}}(\hat{\gamma}_c)]$. Following a procedure similar to the above, one can derive $\nu(\hat{\gamma}_c)$ and $Y(\hat{\gamma}_c)$.

The following makes use of the short-hand notation: $\hat{\nu} = \nu_{\text{syn}}(\hat{\gamma})$ for various critical Lorentz factors; similarly, $\nu_{\text{syn}}(\gamma_0)$ is written ν_0 for commodity.

One can derive the power-law $1 - \beta'$ index of $\nu F_{\nu, \text{syn}}$ as follows. Below ν_c , the scaling remains unchanged compared to the standard case because the cooling history does not influence the synchrotron spectrum, and the results will not be repeated here. Above ν_c , the spectral slope is determined by the scalings of $Y(\gamma)$, $\nu(\gamma)$ and $\nu F_{\nu, \text{syn}} \propto (1+Y)^{-1} \gamma^{2-p}$ [Eq. (12)]. In particular, if $\tilde{\nu}(\gamma)$ lies in a spectral domain in which $\nu F_{\nu, \text{syn}} \propto \nu^{1-\beta}$, below the peak of the synchrotron energy flux, then electrons of Lorentz factor γ cool by inverse Compton interactions with that portion of the synchrotron spectrum if $Y(\gamma) \gg 1$, in which case Eqs. (9), (10) and (11) lead to

$$\begin{aligned} Y &\propto \gamma^{\alpha_t - (1-\beta)(1+\alpha_t)} \\ \nu &\propto \gamma^{2-\beta\alpha_t/2} \\ t_{\text{cool}} &\propto \gamma^{-\beta} \end{aligned} \quad (22)$$

Assuming $\nu F_{\nu, \text{syn}} \propto \nu^{1-\beta'}$ in the range of interest around $\nu(\gamma)$, and using the above scalings, one obtains directly

$$1 - \beta' = \frac{2 - p - \alpha_t + (1 - \beta)(1 + \alpha_t)}{2 - \alpha_t/2 + (1 - \beta)\alpha_t/2}. \quad (23)$$

The limit $\beta \rightarrow 1$ recovers the case in which $\tilde{\nu}$ lies above the peak of the synchrotron flux, discussed previously.

2.4.2 Power-law segments

As mentioned above, the synchrotron spectrum at $\nu < \nu_c$ remains unaffected and it is not discussed here. At the upper end of the spectral range, i.e. $\nu_0 < \nu$, $Y(\gamma) < 1$ because of the Klein-Nishina suppression of electron cooling, which implies that $\nu F_{\nu, \text{syn}} \propto \nu^{1-\beta'}$ with

$$1 - \beta' = \frac{2 - p}{2 - \alpha_t/[2(1 + \alpha_t)]} \quad [\nu_0 < \nu] \quad (24)$$

as can be derived from Eq. (12) with $1 + Y \simeq 1$. This scaling also matches that derived by a full computation of the electron cooling history with negligible inverse Compton losses in Lemoine (2013). For $\alpha_t = 0$, one recovers of course the standard fast cooling index $\beta' = p/2$.

In the range $\hat{\nu}_m < \nu < \nu_0$, if it exists, the synchrotron spectrum is shaped by electrons with Lorentz factor γ such that $\hat{\gamma}_m < \gamma < \gamma_0$, which thus cool by interacting with photons in the range $\nu < \nu_m$; one can therefore use Eq. (23) with $1 - \beta = 4/3$, so that

$$1 - \beta' \simeq \frac{5 - 3p/2 + \alpha_t/2}{3 + \alpha_t/4} \quad (\hat{\nu}_m < \nu < \nu_0) \quad (25)$$

The limit $\alpha_t \rightarrow 0$ gives $\beta' = -2/3 + p/2$, which fits the results of Nakar et al. (2009) in this frequency range.

In the range $\max(\nu_c, \hat{\nu}_c) < \nu < \min(\hat{\nu}_m, \nu_0)$, the Lorentz factor of electrons shaping that part of the spectrum satisfies $\max(\gamma_c, \hat{\gamma}_c) < \gamma < \min(\hat{\gamma}_m, \gamma_0)$, hence one can use Eq. (23) with $1 - \beta = (3 - p)/2$, leading to

$$1 - \beta' \simeq \frac{7 - 3p + (1 - p)\alpha_t}{4 + (1 - p)\alpha_t/2} \quad [\max(\nu_c, \hat{\nu}_c) < \nu < \min(\hat{\nu}_m, \nu_0)] \quad (26)$$

Note that $\hat{\nu}_c < \nu_c$ is equivalent to $\tilde{\nu}_c < \nu_c$. Here as well, one recovers the index $\beta' = -3/4 + 3p/4$ derived in Nakar et al. (2009) in the limit $\alpha_t \rightarrow 0$.

If $\tilde{\nu}_c < \nu_c$, meaning $\hat{\gamma}_c < \gamma_c$, the above completes the description of the spectrum. If, however, $\nu_c < \tilde{\nu}_c$, one needs to describe the intermediate range $\nu_c < \nu < \hat{\nu}_c$. This range can actually be decomposed into two sub-ranges, as follows.

For $\hat{\nu}_c < \nu < \hat{\nu}_c$, the corresponding Lorentz factor verifies $\hat{\gamma}_c < \gamma < \hat{\gamma}_c$, hence $\nu_c < \tilde{\nu} < \hat{\nu}_c$. Consequently, the particle cools on the spectral range of $\nu F_{\nu, \text{syn}}$ that it contributes to through synchrotron emission, so that one can use Eq. (23) with $\beta = \beta'$, giving

$$1 - \beta' \simeq \frac{-2 + 3\alpha_t + [4 + (4 - 8p)\alpha_t + \alpha_t^2]^{1/2}}{2\alpha_t} \quad (\hat{\nu}_c < \nu < \nu_c) \quad (27)$$

and $1 - \beta' \simeq 0.12$ for $\alpha_t = -0.5$, $p = 2.3$, i.e. a slowly rising $\nu F_{\nu, \text{syn}}$.

Finally, in the remaining range $\nu_c < \nu < \hat{\nu}_c$, the particle cools on photons of frequency in the range $\hat{\nu}_c < \tilde{\nu} < \tilde{\nu}_c$, for which $1 - \beta$ is given by Eq. (26) above. This leads to

$$1 - \beta' \simeq \frac{15 - 7p + \alpha_t(1 - p)(10 - p + \alpha_t)/2}{8 + \alpha_t(1 - p)(10 + \alpha_t)/4} \quad (28)$$

One finds $1 - \beta' \simeq 0.09$ for $\alpha_t = -0.5$ and $p = 2.3$.

2.4.3 Inverse Compton component

In principle, one can derive analytical approximations to the inverse Compton component using the above broken power-law approximations, folded over the particle distribution, as in Eq. (17) above. However, this appears rather intricate, given the number of potential power-law segments, in regards of the quality of the approximation that one can obtain; indeed, as discussed in detail in Sari & Esin (2001), folding over the distribution function generally introduces logarithmic departures, which smooth out the power-law segments and breaks. One can nevertheless describe the general features of this inverse Compton component in the slow cooling regime as follows.

Below $\nu_{\text{IC}, m} = 2\gamma_m^2\nu_m$, the slope is that of $\nu F_{\nu, \text{syn}}$ below ν_m , i.e. $4/3$. For $\nu_{\text{IC}, m} < \nu < \nu_{\text{IC}, c}$ with $\nu_{\text{IC}, c} = 2\gamma_c^2\nu_c$, the slope of $\nu F_{\nu, \text{IC}}$ is $(3 - p)/2$, reflecting that of $\nu F_{\nu, \text{syn}}$ in the corresponding range. Above $\nu_{\text{IC}, c}$, the inverse Compton component reflects, up to the afore-mentioned logarithmic corrections, the slope of $\nu F_{\nu, \text{syn}}$ above ν_c , which is generally close to flat or gently rising, see above.

Consequently, if the synchrotron spectrum has an extended range above ν_c where it is close to flat (i.e. $\beta \sim 1$), then one might have a close to flat inverse Compton component, at least up to the cut-off frequency defined as

$$\nu_{\text{IC}, \text{KN}} = \gamma_c^2 \tilde{\nu}_c \quad (29)$$

corresponding the boosting of $\tilde{\nu}_c$ photons at the onset of the Klein-Nishina regime by γ_c electrons. One can define another cut-off frequency, as follows:

$$\nu_{\text{IC},\tilde{\epsilon}} = \hat{\gamma}_c^2 \nu_c \quad (30)$$

which corresponds to the boosting of ν_c photons by electrons of Lorentz factor $\hat{\gamma}_c$, at the onset of the Klein-Nishina regime. The ratio $\nu_{\text{IC},\tilde{\epsilon}}/\nu_{\text{IC,KN}}$ can be written as $\hat{\gamma}_c/\gamma_c$, hence the ordering of one with respect to the other depends on whether $\gamma < \hat{\gamma}_c$ or not. In any case, the actual cut-off occurs at $\nu_{\text{IC,KN}}$, while the presence of $\nu_{\text{IC},\tilde{\epsilon}}$ may lead to a feature (e.g. softening) in the inverse Compton spectrum. This can be understood by noting that in the present case, the synchrotron (energy) flux generically peaks above ν_c , while the particle distribution function falls steeply beyond γ_c , hence the peak of the inverse Compton component is determined by the boosting of $\tilde{\nu}_c$ photons by electrons of Lorentz factor γ_c .

2.4.4 Comparison to numerical calculations

The above analytical broken power-law model of the synchrotron spectrum is compared to a full numerical calculation (with the algorithm described in Sec. 2.5 thereafter) in Fig. 1, in two different representative cases: upper panel, observer time $t_{\text{obs}} = 10^4$ s, blast energy $E = 10^{53}$ ergs, external density $n = 0.01$ cm $^{-3}$; lower panel, $t_{\text{obs}} = 3 \times 10^4$ s, $E = 10^{54}$ ergs, $n = 10^{35} r^{-2}$ cm $^{-3}$ (wind profile with shock radius r expressed in cm); for both, $\epsilon_e = 0.1$, $p = 2.3$, $\epsilon_{B+} = 0.01$ and $\alpha_t = -0.4$, assuming $\epsilon_B = \epsilon_{B+} [t/(100\omega_{\text{pi}}^{-1})]^{\alpha_t}$. For a decelerating adiabatic Blandford & McKee (1976) solution, the value of the blast Lorentz factor at these observer times are $\Gamma_b \simeq 33$ for the upper panel and $\Gamma_b \simeq 29$ in the lower panel. For the above decay law of the magnetic field, one finds for the first scenario $\epsilon_{B-} = 3.2 \times 10^{-5}$ ($t_{\text{dyn}} = 1.3 \times 10^6$ s, $\omega_{\text{pi}}^{-1} = 7.6 \times 10^{-3}$ s), and in the second scenario $\epsilon_{B-} = 2.1 \times 10^{-5}$ ($t_{\text{dyn}} = 1.7 \times 10^6$ s, $\omega_{\text{pi}}^{-1} = 3.5 \times 10^{-3}$ s).

The critical frequencies are indicated with arrows. The thick solid line corresponds to the numerical calculation (synchrotron in blue, inverse Compton component in orange) while the dashed line shows the analytical estimates, which clearly provides a faithful match in both cases.

In the first scenario (upper panel), $\hat{\gamma}_c \simeq 60$ while $\gamma_c \simeq 10^7$: Klein-Nishina effects are therefore particularly strong; there are actually so strong that $\nu_0 < \nu_c$, which means that the Klein-Nishina suppression of electron cooling reduces the Compton parameter to below unity at γ_c . Consequently, the dependence of Y on γ does not affect the spectrum above ν_c . Noting that in this region $\nu F_\nu \propto \gamma^{2-p}$ [Eq. (12)] and $\nu \propto \gamma^{2-\alpha_t/2(1+\alpha_t)}$ [Eq. (10)], one finds $\nu F_\nu \propto \nu^{1-\beta}$ with $1-\beta = (2-p)/[2-\alpha_t/2(1+\alpha_t)]$, which matches Eq. (24). As mentioned earlier, the spectrum remains unaffected with respect to the standard synchrotron spectrum below ν_c because the electrons shaping that part of the spectrum do not cool on a dynamical timescale.

In this first scenario, the method proposed in Eqs. (19) overestimates γ_c by a factor 2.5, hence ν_c by a factor 6 and $\nu_{\text{IC,KN}} = \tilde{\nu}_c \gamma_c^2$ by a factor 2.5 as well. Taking into account this overestimate, the numerical calculation indicates that the suppression of the inverse Compton flux becomes noticeable at a factor ~ 5 below the theoretical value of $\nu_{\text{IC,KN}}$, as calculated with the correct γ_c . As anticipated, the characteristic frequency $\nu_{\text{IC},\tilde{\epsilon}}$ leads to a soft softening in the inverse Compton component, but not to a cut-off.

In the second scenario (lower panel), $\gamma_c < \hat{\gamma}_c$ hence Klein-

Nishina suppression of the inverse Compton cooling becomes effective at $\tilde{\nu}_c$ only. The (analytical) synchrotron spectrum is thus close to flat in the region $\nu_c \lesssim \nu \lesssim \tilde{\nu}_c$, as indicated by Eqs. (28), (27) above, then rising with $1-\beta \simeq 0.14$ corresponding to Eq. (26) above for the range $\tilde{\nu}_c < \nu < \nu_0$, because $\nu_0 < \nu_m$. Above ν_0 , Eq. (24) applies and gives the same high energy spectral slope as for the previous scenario.

In this second case, the analytical calculations underestimate γ_c by a factor 1.8. There is nevertheless a broad satisfactory agreement between the analytical synchrotron spectrum and the numerical calculation.

2.4.5 Comparison to non-decaying scenarios

Figure 2 provides a numerical comparison of the spectra shown in the lower panel of Fig. 1 with two calculations for the same parameters but a homogeneous (non-decaying) turbulence: one in which $\epsilon_B = \epsilon_{B+} = 0.01$, another one in which $\epsilon_B = \epsilon_{B-} = 2.1 \times 10^{-5}$, which corresponds to the value of $\epsilon_B(t_{\text{dyn}})$, i.e. close to the contact discontinuity, in the above decaying micro-turbulence model.

As expected the SSC spectrum with decaying microturbulence merges with that corresponding to uniform ϵ_{B-} at frequencies below ν_c , since electrons of Lorentz factor $\gamma < \gamma_c$ then cool in magnetized turbulences of equal strength in both models. The synchrotron spectrum for decaying micro-turbulence also merges with the synchrotron spectrum for uniform ϵ_{B+} at the highest frequencies, since the cooling time for those emitting electrons becomes shorter than Δ , hence the particles effectively cool in a magnetic field characterized by ϵ_{B+} . However, the integrated powers for these two models differ, because the cooling efficiencies $\sim (\gamma_c/\gamma_m)^{2-p}$ differ.

In this regard, the slow cooling synchrotron spectrum for decaying micro-turbulence is a hybrid of the spectra for uniform high and low ϵ_B , transiting from ϵ_{B-} at low frequencies to ϵ_{B+} at high frequencies. This justifies the use of a two zone model, one with low ϵ_{B-} and one for high ϵ_{B+} , to compute an approximated spectrum in wavebands at respectively low and high frequencies.

In Fig. 2, the synchrotron spectra have been arbitrarily continued at very high frequencies, albeit with a thin line, but they should of course cut-off at some maximal energy where the acceleration timescale becomes of the same order as the cooling timescale. Since this depends on acceleration physics, see the discussion in Lemoine (2013), the lines have been turned from thick to thin at an ad-hoc location corresponding to a synchrotron photon energy of 1 GeV. This estimate is discussed in Plotnikov et al. (2013), Lemoine (2013), Wang et al. (2013), Sironi et al. (2013); it depends on the afterglow parameters and, in particular, on observer time.

For reference, one notes the critical frequencies:

$$\begin{aligned} \nu_{\text{IC},c} &= 2\gamma_c^2 \nu_c \\ &\simeq 7.3 \times 10^{23} \text{ Hz } E_{54} \epsilon_{B-,-5}^{-7/2} A_{*,11.7}^{-9/2} t_{\text{obs},4.5}^2 z_+^{-3} Y_{c,2}^{-4} \\ \nu_{\text{IC,KN}} &= \frac{1}{1+z} \Gamma_b \gamma_c m_e c^2 \\ &\simeq 4 \times 10^{25} \text{ Hz } E_{54}^{1/2} \epsilon_{B-,-5}^{-1} A_{*,11.7}^{-3/2} t_{\text{obs},4.5}^{1/2} z_+^{-3/2} Y_{c,2}^{-1} \end{aligned} \quad (31)$$

with the notations $z_+ = (1+z)/2$, $Y_{c,2} = (1+Y_c)/100$ and $A_{*,11.7} = A_*/(5 \times 10^{11} \text{ g/cm}^2)$. For reference, in the scenario of Figs. 2 and 3, $A_* \simeq 0.3$ and $Y_c \simeq 50$ for $\epsilon_{B-} = 2.1 \times 10^{-5}$. Note the strong dependence of $\nu_{\text{IC},c}$ and ν_{KN} on the external density.

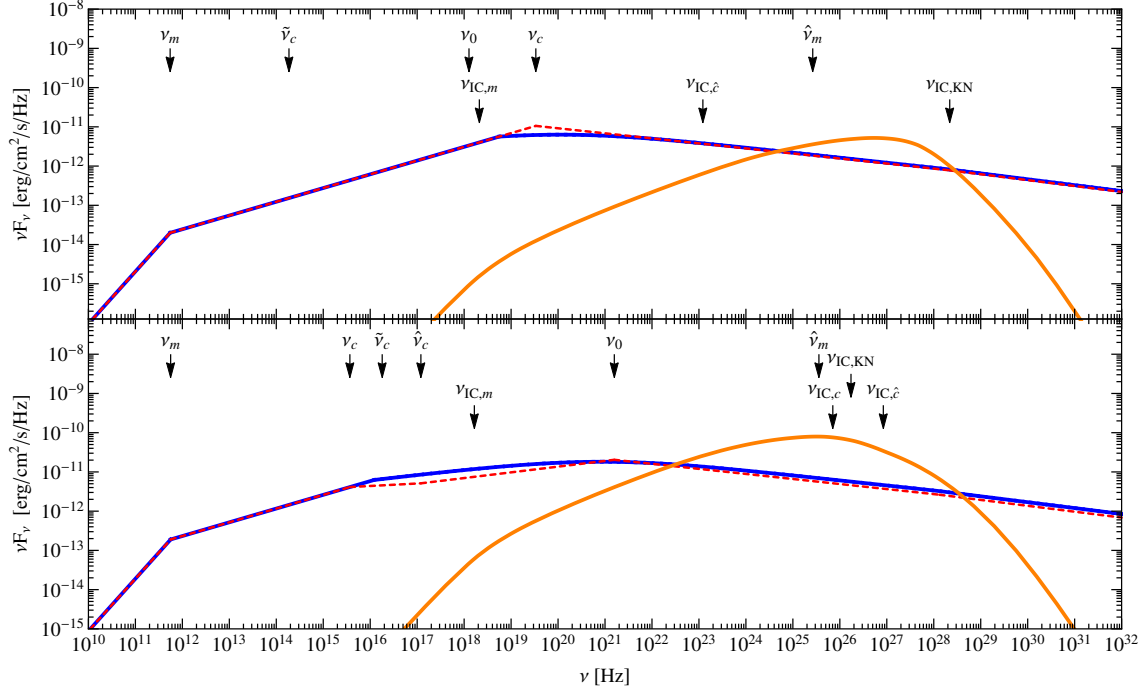


Figure 1. Comparison of the analytical calculation (dashed red line) of the synchrotron spectrum in the slow cooling regime to a numerical calculation (solid blue line), for two representative cases: upper panel, observer time $t_{\text{obs}} = 10^4$ s, blast energy $E = 10^{53}$ ergs, external density $n = 0.01 \text{ cm}^{-3}$; lower panel, $t_{\text{obs}} = 3 \times 10^4$ s, $E = 10^{54}$ ergs, $n = 10^{35} r^{-2} \text{ cm}^{-3}$; in both cases, $\epsilon_e = 0.1$, $p = 2.3$ and $\epsilon_B = \epsilon_{B+} \left[t / (100 \omega_{\text{pi}}^{-1}) \right]^{-0.4}$. The analytical estimates of the characteristic frequencies are indicated with arrows. The solid orange line represents the numerical calculation of the inverse Compton component.

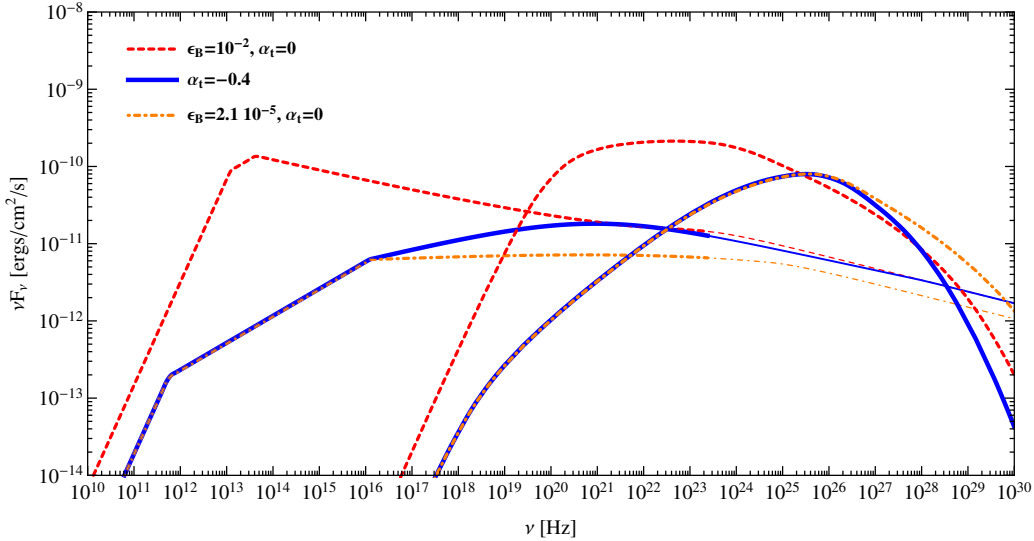


Figure 2. Synchrotron and inverse Compton spectra at $t_{\text{obs}} = 3 \times 10^4$ s, representative of the slow cooling regime, for a blast with energy $E = 10^{54}$ ergs impinging on a progenitor wind with density $n = 10^{35} r^{-2} \text{ cm}^{-3}$ (r in cm), assuming $\epsilon_e = 0.1$ and $p = 2.3$, for three microphysical models, as indicated: homogeneous (non-decaying) $\epsilon_B = \epsilon_{B+} = 0.01$ (dashed red line); decaying $\epsilon_B = \epsilon_{B+} \left[t / (100 \omega_{\text{pi}}^{-1}) \right]^{-0.4}$ (solid blue); homogeneous $\epsilon_B = \epsilon_{B-} = 2.1 \times 10^{-5}$ (dash-dotted orange), the value of ϵ_{B-} being representative of ϵ_B close to the contact discontinuity in the decaying ϵ_B model. The synchrotron model predictions have been thinned beyond an ad-hoc maximal synchrotron photon energy of 1 GeV (see text). Characteristic frequencies are: for $\alpha_t = -0.4$ and for $\epsilon_B = \epsilon_{B-}$, $\nu_m \simeq 5.6 \times 10^{11}$ Hz, $\nu_c \simeq 1.2 \times 10^{16}$ Hz and $\nu_{\text{IC,KN}} \simeq 2 \times 10^{26}$ Hz; for $\epsilon_B = \epsilon_{B+}$, $\nu_m \simeq 1.2 \times 10^{13}$ Hz, $\nu_c \simeq 4.2 \times 10^{13}$ Hz and $\nu_{\text{IC,KN}} \simeq 2 \times 10^{24}$ Hz.

As discussed above, the peak of the inverse Compton component is expected to occur at $\nu_{\text{IC,KN}}$, although the numerical calculation suggests that the turn-over becomes manifest a factor ~ 5 below the above theoretical value.

The VERITAS collaboration has recently been able to observe the exceptional GRB130427A and to put stringent upper limits on the emission at $\gtrsim 100$ GeV (Aliu et al. 2014). The absence of detection of this energy range suggests that, for this burst at least, the inverse Compton component has cut-off below $\simeq 100$ GeV, while the Fermi detection of multi-GeV photons up to a day or so suggests that this cut-off lied above $1 - 10$ GeV. Such a cut-off energy fits well with the above estimates for $\nu_{\text{IC,KN}}$ for a low average ϵ_B .

2.5 Fast cooling

The fast cooling regime involves a substantial variety of synchrotron spectra, with multiple breaks and indices, as discussed in detail in Nakar et al. (2009) and Wang et al. (2010) for the case of uniform ϵ_B . One key difference with the slow-cooling regime is that particles with Lorentz factors $\gamma < \max(\gamma_c, \gamma_m)$ may have a non-trivial cooling history while in the slow-cooling regime, such particles do not cool. As a consequence, it is difficult to even derive the cooling Lorentz factor and the Compton parameter Y_c when Klein-Nishina effects become significant.

In this fast-cooling regime, it is actually more efficient to compute the spectrum numerically, using the following simple and efficient algorithm. One starts with a template synchrotron spectrum, for instance that corresponding to a homogeneous magnetized turbulence. One can then derive a first approximation to γ_c and Y_c , either using standard formulae (e.g Panaitescu & Kumar 2000) – which ignore KN effects – or through an explicit determination of γ_c as the Lorentz factor for which cooling takes place on a dynamical timescale, using a radiation energy density inferred from the template spectrum. With γ_c and Y_c , one can solve Eqs. (9), (10) and (11) to compute the frequencies and Compton parameter as a function of the initial Lorentz factor of an electron; one can then use Eqs. (12) and (13) to compute an improved version of the synchrotron spectrum, properly taking into account the cooling history of the electrons in the decaying turbulence as well as all relevant Klein-Nishina effects. This latter spectrum remains an approximation, because it relies on a guessed value for γ_c and Y_c . Nevertheless, iterating the above process, using each time as a template the previously computed synchrotron spectrum, one obtains after ~ 10 iterations a self-consistent synchrotron spectrum, with γ_c and Y_c determined to high accuracy. Finally, one can derive the inverse Compton spectrum using Eq. (17).

The above algorithm provides a self-consistent estimate of the synchrotron and inverse Compton spectra with a normalization accuracy of order unity. This accuracy can be checked by calculating a posteriori the integrated synchrotron and inverse Compton powers and comparing to the total electron power injected through the shock: in the fast cooling regime, these should match. The error is of order $10 - 40\%$ for the SSC spectrum of a decaying micro-turbulence as shown in Fig. 3, depending on observer time; it is less than $10 - 20\%$ for $\alpha_t = 0$ and $\epsilon_B = \epsilon_{B+}$, but it becomes a factor $\lesssim 2$ for $\alpha_t = 0$ and $\epsilon_B = \epsilon_{B-}$. Most of the error results from the broken power-law normalization of the flux in Eq. (12) and from the treatment of the Klein-Nishina cross-section as a step function in the calculation of the synchrotron cooling history. The resulting uncertainty remains nevertheless satisfactory given the uncertainty associated for instance to the definition of t_{dyn} (hence γ_c) in the absence of a realistic description of the blast energy profile.

A detailed example of the SSC spectrum of the blast, for the same parameters as in Fig. 2, is presented in Fig. 3 at an observer time $t_{\text{obs}} = 30$ s; assuming a Blandford & McKee (1976) decelerating solution in a wind profile, the Lorentz factor of the blast at that time is $\Gamma_b \simeq 160$. The value of ϵ_{B-} in this case is 4.2×10^{-5} . As expected, the spectrum corresponding to a decaying turbulence merges with the spectrum for uniform $\epsilon_B = \epsilon_{B+}$ above a frequency $\nu \sim 10^{23}$ Hz, since the electrons that emit in that range cool fast, in a region where $\epsilon_B \simeq \epsilon_{B+}$. In this fast cooling regime, the total integrated energy densities of the three SSC spectra correspond to the injected electron energy density. The spectrum for decaying micro-turbulence does not merge with that for uniform $\epsilon_B = \epsilon_{B-}$ at low frequencies, since the cooling Lorentz factors differ for both. In this fast cooling regime, one cannot therefore describe accurately the synchrotron spectrum at low frequencies with a spectrum computed for uniform low ϵ_B : an explicit calculation becomes necessary.

Finally, note that the inverse Compton component in the fast cooling regime is expected to peak at $\gamma_m^2 \nu_m$, if the synchrotron flux peaks at ν_m and if one omits KN effects. The Klein-Nishina suppression implies a turn-over of the IC component at most at $\gamma_m^2 \tilde{\nu}_m$, for reasons analog to those discussed in the slow cooling regime, see also Nakar et al. (2009). If $\nu_m < \tilde{\nu}_m$, the slow rise of the synchrotron flux above ν_m in the case of low ϵ_B (due to the KN suppression of electron cooling) or decaying micro-turbulence implies a comparable behavior of the IC component between $\gamma_m^2 \nu_m$ and $\gamma_m^2 \tilde{\nu}_m$. This feature is not clearly seen in Fig. 3 due to the (relative) proximity of these two frequencies, $\gamma_m^2 \tilde{\nu}_m \simeq 6 \times 10^{25}$ Hz and $\gamma_m^2 \nu_m \simeq 10^{24}$ Hz.

3 SPECTRA AND LIGHT CURVES

3.1 Spectral and temporal behaviors

The spectra shown in Figs. 2 and 3 illustrate how a complete and simultaneous spectral coverage would allow to tomograph the evolution of the micro-turbulence behind the relativistic shock. The effects are most noticeable in the X-ray and MeV regions, as one would expect: in this region of the spectrum, the emitting electrons feel the decaying turbulence, while at the highest frequencies, they cool in regions with $\epsilon \sim \epsilon_{B+}$, and at frequencies $\nu < \nu_c$ they cool in a magnetic field characterized by ϵ_{B-} , the value of which evolves slowly in time.

Afterglow models often rely on the spectral and temporal slopes in various domains and their so-called closure relations to make comparison to observations. Figure 4 therefore presents the spectral slopes β defined by $F_\nu \propto \nu^{-\beta}$ (where F_ν sums the synchrotron and inverse Compton fluxes), for the optical, X-ray, high energy ($0.1 - 10$ GeV) and very high energy (> 10 GeV) ranges (note that no attenuation in extra-galactic background radiation has been assumed for the latter range). This figure compares the spectral slopes for the three previous representative models: ($\alpha_t = 0$, $\epsilon_B = 0.01$), ($\alpha_t = -0.4$) and ($\alpha_t = 0$, $\epsilon_B = 10^{-5}$) with otherwise same parameters as in Figs. 2, 3, except k , which takes values 0 (constant density profile) or 2 (stellar wind).

In the optical, β has been calculated at a reference frequency of 4.7×10^{14} Hz (R band); in the X-ray, β is calculated as the average slope over the interval of energies $0.3 - 10$ keV; at high energy, it is calculated as the average of the energy interval $0.1 - 10$ GeV and at very high energy, over > 10 GeV.

According to Fig. 4, the most robust signature of a decaying micro-turbulence appears to be a slightly harder slope in the

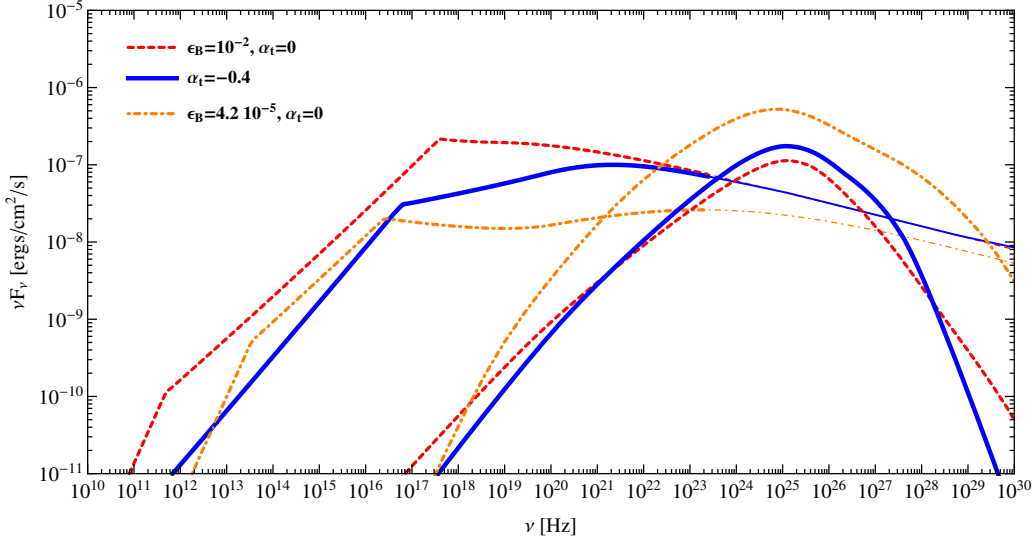


Figure 3. Same as Fig. 2 at observer time $t_{\text{obs}} = 30$ s, representative of the fast cooling regime. Characteristic frequencies are: for $\alpha_t = -0.4$, $\nu_c \simeq 10^{12}$ Hz, $\nu_m \simeq 3 \times 10^{16}$ Hz and $\gamma_m^2 \tilde{\nu}_m \simeq 6 \times 10^{25}$ Hz; for $\epsilon_B = \epsilon_{B-}$, $\nu_c \simeq 2 \times 10^{13}$ Hz, $\nu_m \simeq 3 \times 10^{16}$ Hz and $\gamma_m^2 \tilde{\nu}_m \simeq 6 \times 10^{25}$ Hz; for $\epsilon_B = \epsilon_{B+}$, $\nu_c \simeq 4 \times 10^{11}$ Hz, $\nu_m \simeq 4 \times 10^{17}$ Hz and $\gamma_m^2 \tilde{\nu}_m \simeq 6 \times 10^{25}$ Hz.

X-ray, $\beta \simeq 0.9$ [panels (b) and (e)] vs $\beta \simeq 1.15$ for uniform ϵ_B in the first hours [panels (a), (c), (d) and (f)]. The latter value corresponds to the fast cooling regime $\beta = p/2$, therefore it depends on p ; however, one does not expect it to go below 1, because $p > 2$ is a generic prediction of relativistic shock acceleration, e.g. Bednarz & Ostrowski (1998), Kirk et al. (2000), Achterberg et al. (2001), Lemoine & Pelletier (2003), Sironi et al. (2013). Current data do not allow to distinguish between these limits; in particular, the Swift data lead to $\beta \simeq 1 \pm 0.1$ (Evans et al. 2009) in afterglows with standard power-law decay. Interestingly, even in the case of a homogeneous turbulence, the X-ray slope hardens at late times because of the emergence in the X-ray range of the inverse Compton component; for instance, in panels (a) and (c), one can see β transit to values of order 0.7, corresponding to the low energy extension of this inverse Compton component with slope $\beta = (p-1)/2$.

In the optical range, the slope is comparable to that in the X-ray range for the decaying micro-turbulence scenario at observer times $\sim 10^3$ s, but significantly harder at earlier times when the optical falls in the range $\nu_c - \nu_m$: Fig. 4 indicates values $\beta \sim 0.3$, harder than expected ($1/2$) in the standard fast cooling regime in this range of frequencies. At an observer time $t_{\text{obs}} = 30$ s, for $k = 2$ corresponding to panel (e) as well as to Fig. 3, $\tilde{\nu}_m \simeq 1.4 \times 10^{18}$ Hz, which lies below the peak of the synchrotron component (see Fig. 3). This implies that Klein-Nishina effects are significant, and that γ_m electrons cool by interacting with the segment in the range $10^{17} - 10^{21}$ Hz, whose index $\beta \sim 0.8$. In this case, one can compute the expected index β' of the segment below ν_m , using a variant of Eq. (23): one notes that $\nu F_{\nu, \text{syn}} \propto \gamma/(1+Y)$ [Eq. (13)], which gives

$$1 - \beta' = \frac{1 - \alpha_t + (1 - \beta)(1 + \alpha_t)}{2 - \alpha_t/2 + (1 - \beta)\alpha_t/2} \simeq 0.3 \quad (32)$$

the last equality applying for $\alpha_t = -0.4$ and $\beta = 0.8$. This explains the values of α_t found in the optical range. Such values do depart from the standard synchrotron spectra, although Klein-Nishina effects may also cause values $\beta \sim 0.3$ below ν_{min} in the case of homogeneous turbulence scenarios, see Nakar et al. (2009), their figures 2 and 3 for example. Therefore, it is not clear at present

whether one can consider such values of β as a clear signature of a decaying micro-turbulence.

All in all, an accurate measurement of β in the X-ray range, or better, in the MeV range if the MeV afterglow could be detected, would provide the best probe of α_t , see also Fig. 2 and 3 for illustrations of these effects.

Another quantity of interest for a general description of the afterglow is the temporal slope, defined by $F_\nu \propto t_{\text{obs}}^{-\alpha}$. Of course, these temporal slopes directly depends on the time evolution of the various parameters, through the assumed evolutionary law for Γ_b and the evolution of r and n , in contrary to the spectral slopes β at any given time. Here Γ_b is assumed to decrease as in the Blandford & McKee (1976) adiabatic solution, i.e. $\Gamma_b \propto t^{(k-3)/[2(4-k)]}$.

The values of α for the same models and intervals as Fig. 4 are reported in Fig. 5. The largest differences between constant (high) and decaying ϵ_B result from the different transit times between the slow and fast cooling regimes, but these times depend in turn on other parameters that are a priori unknown. The light curves otherwise present similar features, without a clear trend distinguishing one from the other.

Figures 4 and 5 thus indicate that α and β are by themselves weakly sensitive probes of the dynamics of the magnetized turbulence in the blast and that it is not possible at present to distinguish a decaying micro-turbulence from a uniform low- or high ϵ_B on the basis of these data. It appears much more effective to try to probe ϵ_B through a multiwavelength fit of the afterglow light curves, using not only the temporal and spectral slopes, but also the ratio of fluxes between different spectral windows, as done in Lemoine et al. (2013), Liu et al. (2013) for Fermi-LAT bursts.

3.2 Emission at very high energy

Finally, an interesting consequence of a decaying micro-turbulence is the generic prediction of substantial emission at the highest energies, due to the large value of the Compton parameter. Naive estimates, $Y \sim \sqrt{\epsilon_e/\epsilon_{B-}}$, indicate values of several hundreds for Y , although they neglect Klein-Nishina effects which depend on the electron energy, therefore on observed frequency; further-

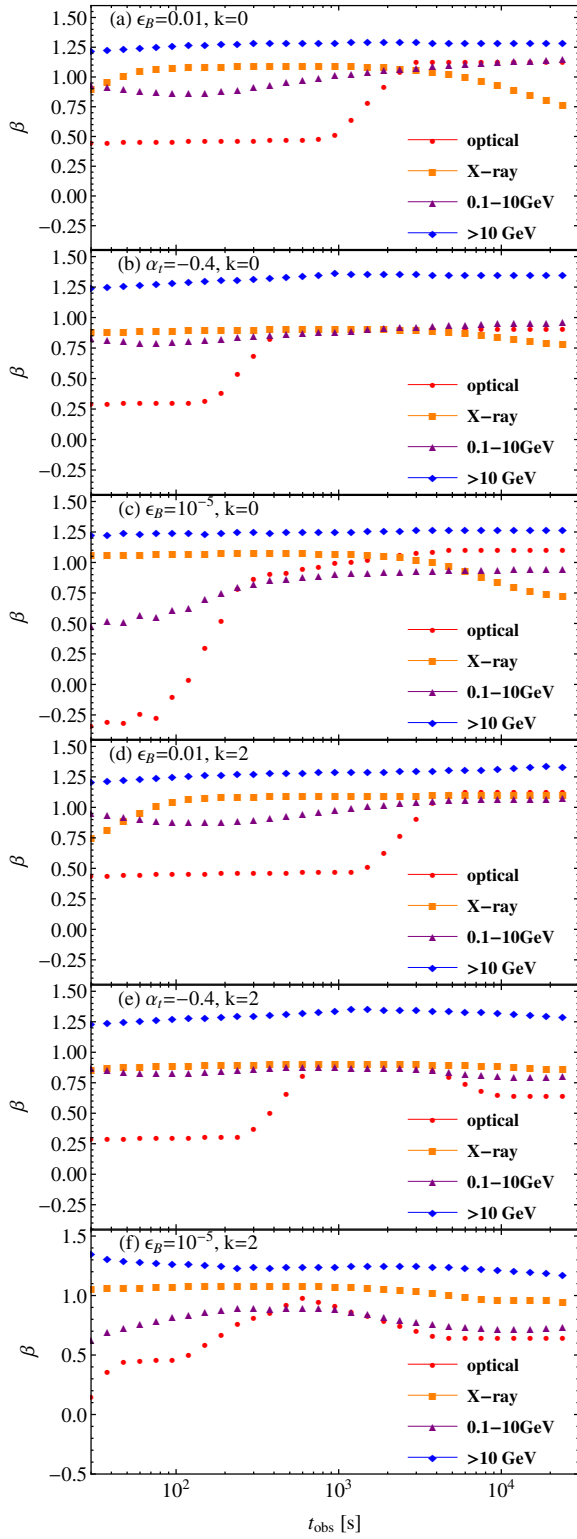


Figure 4. Flux density index β , with $F_\nu \propto \nu^{-\beta}$, as a function of time, in various wavebands, for different external density profiles: $k=2$ (wind, $n=10^{35} r^{-2} \text{ cm}^{-3}$) and $k=0$ (constant density, $n=1 \text{ cm}^{-3}$), assuming uniform $\epsilon_B=0.01$, $\epsilon_B=(100\omega_{\text{p}i}t)^{\alpha_t}$ or uniform $\epsilon_B=10^{-5}$. Blast energy, jet Lorentz factor and ϵ_e are as in Fig. 2. Wavebands are as indicated: for reference, optical (circles) $\nu=4.7 \times 10^{14}$ Hz, X-ray (squares) integrated from 0.3 to 10 keV (i.e. $0.72-24 \times 10^{17}$ Hz), 0.1-10 GeV (upward triangles, in frequency $0.24-24 \times 10^{23}$ Hz) and >10 GeV (diamonds, in frequency $>24 \times 10^{23}$ Hz).

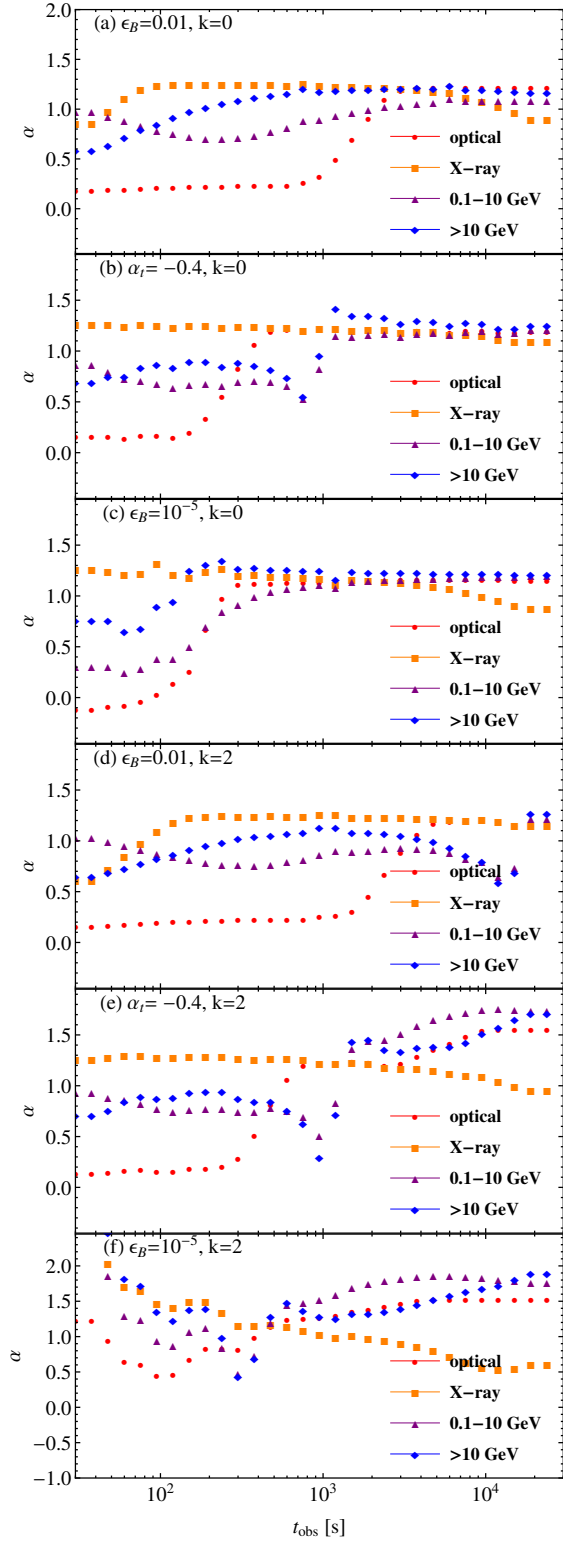


Figure 5. Observer time decay index of the flux density, i.e. $F_\nu \propto t_{\text{obs}}^{-\alpha}$, for various models, as indicated in Fig. 4. Blast energy and ϵ_e are as in Fig. 2.

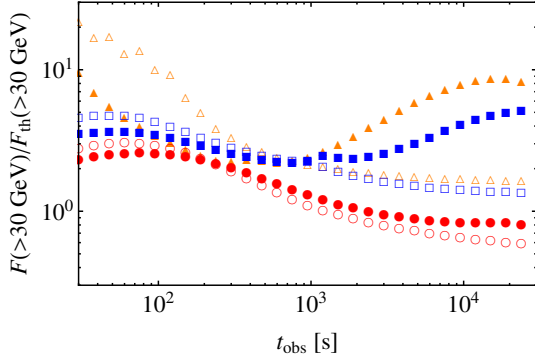


Figure 6. Ratio of the total energy flux above 30 GeV to a theoretical flux obtained by matching the calculated total flux at 0.1 GeV and extrapolating this flux to higher energies with a power-law $F_{\nu,th} \propto \nu^{-1.1}$, as in Inoue et al. (2013). The symbols correspond to the six models studied in Figs. 4 and 5, as follows: red circles $\epsilon_B = \epsilon_{B+}$ and $\alpha_t = 0$; blue squares $\alpha_t = -0.4$; orange triangles $\epsilon_B = \epsilon_{B-}$ and $\alpha_t = 0$. Filled symbols correspond to $k = 2$ and open symbols to $k = 0$; other parameters are as in Fig. 2.

more, the non-trivial spectral shape above ν_c in the case of decaying micro-turbulence modifies the ratio of the inverse Compton to the synchrotron component. As discussed in Wang et al. (2013), emission above 10 GeV is most likely of inverse Compton origin, because the maximal synchrotron photon energy is more likely of the order of 1 GeV or so at 100 – 1000 sec observer time. This emission is a prime target for future gamma-ray telescopes such as HAWK (Mostafa 2013) or CTA (Inoue et al. 2013). For the particular case of CTA, Inoue et al. (2013) have investigated the detection rates of gamma-ray bursts above 30 GeV by assuming that the spectrum continues beyond 1 GeV with a spectral index $\beta = 1.1$ (corresponding to the standard fast cooling regime $\beta = p/2$ with $p = 2.2$) and scaling the flux at 1 GeV to that measured by the Fermi-LAT instruments. Their simulations lead to about one detection per year. This rate is rather low, therefore any improvement would be quite valuable, given the potential impact of a high energy detection.

One can use the calculations of Sec. 2 to study how a decaying micro-turbulence or low ϵ_{B-} affects these predictions. In order to do so, one calculates the ratio of the total (synchrotron + inverse Compton) energy flux above 30 GeV, $F(> 30 \text{ GeV}) = \int_{30 \text{ GeV}} F_\nu d\nu$ to a theoretical reference flux $F_{th}(> 30 \text{ GeV})$. As in Inoue et al. (2013), $F_{th}(> 30 \text{ GeV})$ is obtained by extrapolating the total flux measured at a reference energy, here 0.1 GeV, with an index $\beta \simeq 1.1$, i.e.

$$F_{th}(> 30 \text{ GeV}) = F_\nu(0.1 \text{ GeV}) \times \int_{30 \text{ GeV}/h}^{+\infty} d\nu \left(\frac{h\nu}{0.1 \text{ GeV}} \right)^{-1.1} \quad (33)$$

with $F_\nu = F_{\nu,syn} + F_{\nu,IC}$ the total flux. The reference energy chosen here is smaller than that in Inoue et al. (2013), because the inverse Compton flux is already prominent at 1 GeV in the scenarios studied, as shown in Fig. 2 and 3 for example. However, given the value of the index β , the theoretical flux νF_ν is roughly flat above 1 GeV, hence this should not affect the statistics of detection.

The results are shown in Fig. 6, which carries out this evaluation for the six models shown in Figs. 4 and 5. This figure indicates

that a decaying micro-turbulence with $\alpha_t = -0.4$ (or a low average ϵ_B) increases by a factor of a few, up to an order of magnitude, depending on α_t , k and t_{obs} , the prospects of observing the afterglows at energies $> 30 \text{ GeV}$, relatively to statistics computed for a model with $\epsilon_B = 0.01$, as in Inoue et al. (2013). This certainly brings the number of potential detections by instruments such as CTA in a more comfortable range.

Furthermore, it is important to note that in most models studied here, the inverse Compton component contributes to a significant fraction of the total flux at 0.1 GeV, therefore the above ratio actually is an underestimate of the ratio of the inverse Compton flux at high energies to the synchrotron flux at GeV energies.

4 CONCLUSIONS

This paper has discussed the spectral shapes of the synchrotron-self-Compton spectrum of a relativistic blast wave, including all relevant Klein-Nishina effects, and their evolution in time. A particular emphasis has been put on the impact of a decaying micro-turbulence behind the shock front, which is motivated by theoretical analysis (Chang et al. 2008, Lemoine 2015) and observational inference (Lemoine et al. 2013, Liu et al. 2013). However, the results are fully applicable to the case of a uniformly magnetized blast, possibly with a low value of the average ϵ_B .

A decaying micro-turbulence and/or a low average value of ϵ_B both lead to a large Y_c Compton parameter, with interesting physical and observational consequences. From a more theoretical point of view, the Klein-Nishina suppression of inverse Compton cooling has a strong effect on the synchrotron spectral shape, as noted elsewhere for the case of a uniformly magnetized blast (Nakar et al. 2009, Wang et al. 2010). In the case of a decaying micro-turbulence, the modification is not trivial to compute, and the present paper has described a simple algorithm which allows to compute the full SSC spectrum with satisfactory accuracy, at a modest numerical cost. Among the interesting phenomenological consequences, one may point out the slight deviations in the spectral and temporal slopes induced by the decaying micro-turbulence, or by KN effects in uniformly magnetized blasts at low ϵ_B . A multi-wavelength coverage of the afterglow would, in principle, allow one to tomograph the dynamics of this magnetized turbulence, through its influence on the light curves in various wavebands. However, as expressed in terms of the spectral β and temporal α slopes, defined customarily through $F_\nu \propto t_{obs}^{-\alpha} \nu^{-\beta}$, the deviations are relatively weak and not currently distinguishable through observations. A multiwavelength fit of the afterglow, which also relies on the flux ratios between various wavebands, seems to provide a more sensitive probe of the dynamics of the micro-turbulence.

Finally, a large Y_c parameter also implies a large inverse Compton flux at multi-GeV energies, relatively to the lower energy synchrotron flux, with direct consequences for the detectability of gamma-ray bursts afterglows by future gamma-ray telescopes. A numerical estimate indicates that a low average ϵ_B would imply a detection rate several times larger than currently anticipated on the basis of the extrapolation of the flux of gamma-ray bursts detected by Fermi-LAT.

Acknowledgments: An anonymous referee is acknowledged for helpful suggestions; H. He is acknowledged for discussions. This work has been financially supported by the Programme National Hautes Énergies (PNHE) of the C.N.R.S. and by the ANR-14-CE33-0019 MACH project.

REFERENCES

- Achterberg, A., Gallant, Y. A., Kirk, J. G., Guthmann, A. W., 2001, MNRAS, 328, 393
- Achterberg, A., Wiersma, J., 2007, AA, 475, 19
- Achterberg, A., Wiersma, J., Norman, C. A., 2007, AA, 475, 1
- Aliu, E. et al. (VERITAS Collaboration), 2014, ApJ, 795, L3
- Barniol-Duran, R., Kumar, P., 2011, MNRAS, 417, 1584
- Barniol-Duran, R., 2014, MNRAS, 443, 3578
- Bednarz, J., Ostrowski, M., 1998, Phys. Rev. Lett., 80, 3911
- Blandford, R. D., McKee, C. F., 1976, Phys. Fluids, 19, 1130
- Blumenthal, G. R., Gould, R. J., 1970, Rev. Mod. Phys., 42, 237
- Bošnjak, Ž., Daigne, F., Dubus, G., 2009, AA, 498, 677
- Bret, A., Gremillet, L., Bénisti, D., 2010, Phys. Rev. E, 81, 036402
- Chang, P., Spitkovsky, A., Arons, J., 2008, ApJ, 674, 378
- Daigne, F., Bošnjak, Ž., Dubus, G., 2011, AA, 526, 110
- Derishev, E., 2007, Astrophys. Sp. Sc., 309, 157
- Evans, P. A. et al. (Swift-XRT), 2009, MNRAS, 397, 1177
- Gruzinov, A., Waxman, E., 1999, ApJ, 511, 852
- Haugbølle, T., 2011, ApJ, 739, 42
- He, H.-N., Wu, X.-F., Toma, K., Wang, X.-Y., Mészáros, P., 2011, ApJ, 733, 22
- Inoue, S. et al. (CTA Collaboration), 2013, Astropart. Phys., 43, 252
- Kato, T. N., Takabe, H., 2008, ApJ, 681, L93
- Keshet, U., Katz, B., Spitkovsky, A., Waxman E., 2009, ApJ, 693, L127
- Kirk, J., Guthmann, A. W., Gallant, Y., Achterberg, A., 2000, ApJ, 542, 235
- Kirk, J., Reville, B., 2010, ApJ, 710, 16
- Kumar, P., Barniol-Duran, R., 2009, MNRAS, 400, L75
- Kumar, P., Barniol-Duran, R., 2010, MNRAS, 409, 226
- Lemoine, M., Pelletier, G., 2003, ApJ, 589, L73
- Lemoine, M., Pelletier, G., Revenu, B., 2006, ApJ, 645, L129
- Lemoine, M., Pelletier, G., 2010, MNRAS, 402, 321
- Lemoine, M., Pelletier, G., 2011, MNRAS, 417, 1148
- Lemoine, M., 2013, MNRAS, 428, 845
- Lemoine, M., Li, Z., Wang, X.-Y., 2013, MNRAS, 435, 3009
- Lemoine, M., Pelletier, G., Gremillet, L., Plotnikov, I., 2014a, Europhys. Lett., 106, 55001
- Lemoine, M., Pelletier, G., Gremillet, L., Plotnikov, I., 2014b, MNRAS, 440, 1365
- Lemoine, M., 2015, J. Plasma Phys., 81, 455810101
- Liu, R.-Y., Wang, X.-Y., Wu, X.-F., 2013, ApJ, 773, L20
- Lyubarsky, Y., Eichler, D., 2006, ApJ, 647, L1250
- Martins, S. F., Fonseca, R. A., Silva, L. O., Mori, W. B., 2009, ApJ, 695, L189
- Medvedev, M. V., Loeb, A., 1999, ApJ, 526, 697
- Moiseev, S. S., Sagdeev, R. Z., 1963, J. Nucl. Energy, 5, 43
- Mostafa, M. (HAWK Collaboration), 2013, arXiv:1310.7237, 33rd ICRC Conference (Rio de Janeiro, Brazil)
- Nakar, E., Ando, S., Sari, R., 2009, ApJ, 703, 675
- Niemiec, J., Ostrowski, M., Pohl, M., 2006, ApJ, 650, 1020
- Nishikawa, K.-I., Niemiec, J., Hardee, P. E., Medvedev, M., Sol, H., Mizuno, Y., Zhang, B., Pohl, M., Oka, M., Hartmann, D. H., 2009, ApJ, 698, L10
- Panaitecu, A., Kumar, P., 2000, ApJ, 543, 66
- Pelletier, G., Lemoine, M., Marcowith, A., 2009, MNRAS, 393, 587
- Piran, T., 2004, Rev. Mod. Phys., 76, 1143
- Plotnikov, I., Pelletier, G., Lemoine, M., 2013, MNRAS, 430, 1208
- Rabinak, I., Katz, B., Waxman, E., 2011, ApJ, 736, 157
- Rossi, E., Rees, M. J., 2003, MNRAS, 339, 881
- Santana, R., Barniol-Duran, R., Kumar, P., 2014, ApJ, 785, 29
- Sari, R., Piran, T., Narayan, R., 1998, ApJ, 497, L17
- Sari, R., Esin, A. A., 2001 ApJ, 548, 787
- Shaisultanov, R., Lyubarsky, Y., Eichler, D., 2012, ApJ, 744, 182
- Sironi, L., Spitkovski, A., 2009, ApJ, 698, 1523
- Sironi, L., Spitkovski, A., 2011, ApJ, 726, 75
- Sironi, L., Spitkovski, A., Arons, J., 2013, ApJ, 771, 54
- Spitkovsky, A., 2008a, ApJ 673, L39
- Spitkovsky, A., 2008b, ApJ 682, L5
- Wang, X.-Y., He, H.-N., Li, Z., Wu, X.-F., Dai, X.-G., 2010, ApJ, 712, 1232
- Wang, X.-Y., Liu, R., Lemoine, M., 2013, ApJ, 771, L33
- Wiersma, J., Achterberg, A., 2004, AA, 428, 365